JOURNAL OF GEOPHYSICAL RESEARCH, VOL. 112, C12022, doi:10.1029/2006JC003987, 2007

Click Here for Full Article

Density-dependent variations of the along-isobath flow in the East Greenland Current from Fram Strait to Denmark Strait

Pawel Schlichtholz[1]

Received 27 October 2006; revised 18 June 2007; accepted 2 October 2007; published 29 December 2007.

[1] The East Greenland Current (EGC) dynamically connects the Arctic Ocean to the North Atlantic on the western side of the Nordic Seas. Observations show that the speed of the EGC considerably varies along the East Greenland Slope (EGS). Here it is shown, using current meter data reported in the literature and climatological hydrographic fields, that velocity and transport variations along the EGS are supported by the cross-isobath component of the density-dependent geostrophic flow relative to the bottom. The relative flow impinging on (leaving) the EGS in a northern (southern) limb of the cyclonic circulation in the Nordic Seas strengthens (weakens) the along-isobath bottom geostrophic flow. Variations of the latter are clearly associated with along-isobath bottom density gradients. Current observations indicate an increase of the along-isobath bottom velocity from 79°N to 75°N equal to about 9 and 10 cm s^{-1} on the upper (1000 m isobath) and lower (2000 m isobath) EGS, respectively. Corresponding estimates based on bottom density distribution along the 1000 and 2000 m isobaths are grossly consistent with the observations given above though we obtain a higher increase (13 cm s^{-1}) at 1000 m and lower increase (6 cm s^{-1}) at 2000 m. Considering the variability of the system and the poor resolution of the observations we find this to be a very convincing result, demonstrating the power of the geostrophic approximation for such estimates.

Citation: Schlichtholz, P. (2007), Density-dependent variations of the along-isobath flow in the East Greenland Current from Fram Strait to Denmark Strait, *J. Geophys. Res.*, *112*, C12022, doi:10.1029/2006JC003987.

1. Introduction

[2] The Nordic (Greenland-Iceland-Norwegian) Seas (Figure 1) have long been recognized to be a key area for the thermohaline circulation of the World Ocean [e.g., *Gordon*, 1986; *Mauritzen*, 1996a]. In this area, a dense water production occurs as a response to extreme surface heat losses in the cyclonic subpolar (Greenland Sea) gyre and cooling of Atlantic Water (AW) in the Norwegian Atlantic Current (NwAC) - West Spitsbergen Current (WSC) system. The AW, modified in the NwAC-WSC system and then all around the Arctic Ocean, returns to the Nordic Seas on the western side of Fram Strait. This Arctic AW together with the overlying Polar Surface Water and sea ice as well as the underlying deep waters, formed by the boundary convection on the Arctic Ocean shelves and slopes [e.g., *Aagaard et al.*, 1985], are carried southward by the East Greenland Current (EGC). On their way toward the North Atlantic, the water masses of the EGC interact with the Nordic Seas water masses [*Rudels et al.*, 2002, 2005]. Already in Fram Strait some AW is recirculated by the Return Atlantic Current (RAC) and mixed into the EGC [e.g., *Schlichtholz and Houssais*, 1999b]. Further south the dense Arctic Intermediate Water from the open sea convection in the Greenland Sea gyre is also mixed into the EGC. The deepest water masses outflowing from the Arctic Ocean mix with the densest product of the convection in the Greenland Sea gyre, the Greenland Sea Deep Water [e.g., *Aagaard et al.*, 1991]. Some Arctic Intermediate Water is also formed in the Iceland Sea. It interacts with these water masses of the EGC which cross the Jan Mayen Fracture Zone at ~72°N and contribute to the Denmark Strait overflow renewing the deep waters of the World Ocean. Water masses which are too deep to cross the sill at 640 m in Denmark Strait are deflected eastward along the Greenland-Scotland Ridge. Their shallower components may contribute to the overflow feeding the deep waters of the World Ocean in the Faroe Bank Channel (sill at 850 m) while the remainder should participate in the internal circulation of the Nordic Seas.

[3] A cyclonic motion in the Nordic Seas is clearly seen, for instance, in drifter data [*Jakobsen et al.*, 2003]. The circulation is traditionally thought to be mainly driven by a positive wind stress curl in the area. A northward wind-driven transport should be compensated by a southward transport in the EGC playing the role of a return boundary current. *Aagaard* [1970] and *Jónsson* [1991] obtained an annual mean flat-bottom Sverdrup transport of 35 Sv (1 Sv = 10^6 m^3 s^{-1}), in agreement with an estimate of the EGC transport based on observations from a drifting ice island

[1]Institute of Oceanology, Polish Academy of Sciences, Sopot, Poland.

Copyright 2007 by the American Geophysical Union.
0148-0227/07/2006JC003987$09.00

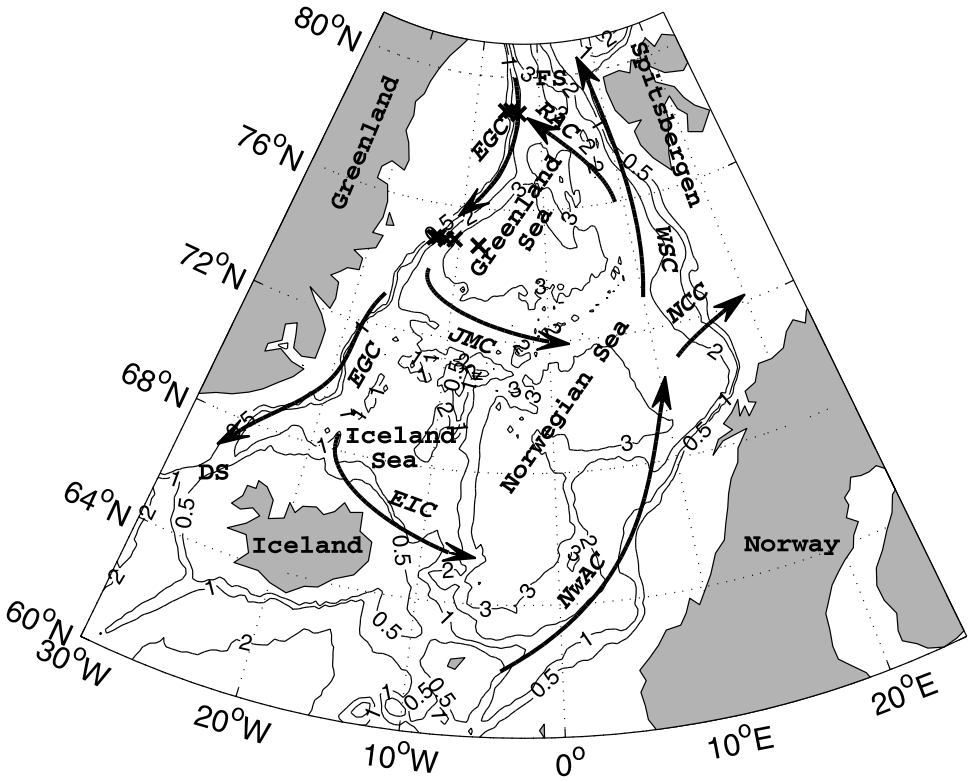

Figure 1. Bottom topography (in km) of the Nordic Seas. The crosses indicate location of moorings at 79°N [*Foldvik et al.*, 1988] and 75°N [*Woodgate et al.*, 1999]. The arrows are schematic representation of the following currents: EGC, East Greenland Current from Fram Strait (FS) to Denmark Strait (DS); NwAC, Norwegian Atlantic Current; NCC, North Cape Current; WSC, West Spitsbergen Current; RAC, Return Atlantic Current; JMC, Jan Mayen Current; and EIC, East Icelandic Current.

[*Aagaard and Coachman*, 1968]. These estimates are larger than the annual mean transport of 21 Sv in the EGC reported by *Woodgate et al.* [1999] from a current meter section occupied from summer 1994 to summer 1995 at 75°N (Figure 1). Calculations made by these authors show that only 14 Sv of the observed annual mean transport can be attributed to the flat-bottom Sverdrup dynamics (estimate for the most relevant choice of the drag coefficient). The difference probably represents a density-driven throughflow from the Arctic Ocean to the North Atlantic. The outflow through Denmark Strait is up to only ~6 Sv [*Hansen and Østerhus*, 2000] while an upper ocean (0–700 m) inflow through Fram Strait is 7 Sv according to the yearlong (summer 1984 to summer 1985) current meter measurements in the EGC at 79°N (Figure 1) carried out by *Foldvik et al.* [1988]. A large transport in the EGC is therefore an intrinsic feature of the Nordic Seas. Even the total inflow through Fram Strait of 12–13 Sv reported by *Schauer et al.* [2004] from recent measurements at 79°N is considerably smaller than the EGC transport at 75°N.

[4] A cyclonic motion in the Nordic Seas can also be deduced from maps of the dynamic height determined from density distributions [e.g., *Metclaf*, 1960]. However, such maps are merely illustrations of a horizontal structure of the vertically sheared geostrophic flow at a chosen depth level referenced to the flow at a deeper level. The flow at the reference level may not be negligible and its determination is a classical problem in physical oceanography [e.g., *Wunsch*, 1996]. Some diagnostic models choose the flow at the ocean bottom as the unknown of the ocean circulation problem [e.g., *Park and Guernier*, 2001; *Nøst and Isachsen*, 2003]. In the Nordic Seas, a considerable depth-independent flow is a remarkable feature of both the NwAC-WSC system and the EGC as demonstrated by diagnostic models [*Schlichtholz and Houssais*, 1999a; *Nøst and Isachsen*, 2003] as well as observations [e.g., *Foldvik et al.*, 1988; *Woodgate et al.*, 1999; *Orvik et al.*, 2001; *Fahrbach et al.*, 2001].

[5] Density gradients are an important dynamical agent since not only they determine the vertical shear of the geostrophic flow, but also contribute to the bottom geostrophic flow wherever the ocean bottom is sloping. The latter contribution is associated with along-isobath variations of the bottom density as emphasized in several studies on slope currents [e.g., *Shaw and Csanady*, 1983; *Csanady*, 1988]. The link between the bottom flow and density has recently been elucidated in a particularly elegant manner by *Walin et al.* [2004] and *Nilsson et al.* [2005]. In particular, *Walin et al.* [2004] suggested, using theoretical considerations and numerical simulations, that a reasonably strong cyclonic circulation could exist in the Nordic Seas even in the absence of wind-forcing. The circulation could be maintained by the inflow of AW across the Greenland-Scotland Ridge and a downstream buoyancy loss due to the heat exchange with the atmosphere.

[6] The influence of density gradients on the depth-independent flow in the Nordic Seas has also been evidenced in a series of papers on the dynamics of the EGC along the East Greenland Slope (EGS) in Fram Strait

based on theoretical considerations and hydrographic data. First, the depth-independent flow in this area was linked to along-isobath variations of the potential energy estimated using quasi-synoptic data from the MIZEX 84 experiment [*Schlichtholz and Houssais*, 1999c]. The MIZEX 84 data were then used to emphasize the role of the bottom density variations along the EGS north of ~77.5°N [*Schlichtholz*, 2002]. The latter were found to be highly correlated with the corresponding variations of the bottom flow obtained from an inverse model published earlier [*Schlichtholz and Houssais*, 1999a]. Finally, it was argued, using climatological data from the PHC (Polar Science Center Hydrographic Climatology [*Steele et al.*, 2001]), that also the mean density field implies a downstream increase of the magnitude of the bottom flow along the EGS in Fram Strait [*Schlichtholz*, 2005].

[7] Here it is shown, using the PHC climatology and published current meter data, that the depth-independent flow in the EGC is likely to be controlled by along-isobath density variations from Fram Strait to Denmark Strait. The study is organized as follows. First, in section 2, velocity and transport changes along the EGS from 79°N to 75°N are estimated from current measurements. Then, in section 3, equations for geostrophic flow are given. Variations of geostrophic flow along the EGS from 79°N to 69°N determined from the density distribution are reported in section 4. The results are discussed and summarized in section 5.

2. Velocity and Transport Estimates From Current Meter Arrays

[8] To illustrate velocity changes along the EGS, estimates of the annual mean flow at 79°N [*Foldvik et al.*, 1988, Table 2] and 75°N [*Woodgate et al.*, 1999, Table 1] are used. At 79°N, moorings named FS-1, FS-2, and FS-3 were located in the water depth (H) of 1094, 1678, and 2359 m, respectively. The lowest instrument at FS-1 and FS-3 (FS-2) was placed 25 (300) m above the bottom (Figures 2a and 2b). At 75°N, four moorings numbered 410-2, 411-2, 412-4, and 413-4 were located on the EGS, in the water depth of 413, 985, 2240, and 3022 m, respectively, and one mooring (414-3) in the Greenland Basin. The lowest instrument at the three westernmost moorings was placed 52 m above the bottom and nearly so at the other two moorings (Figures 2c and 2d). Figure 2 shows distributions of the flow components in the along-isobath (y) direction, v, and the cross-isobath (x) direction, u. The components are obtained by projecting the observed mean velocity, $\mathbf{u}$, on the local bottom depth gradients estimated from the 5-min gridded Earth topography, ETOPO5 [*U.S. National Geophysical Data Center*, 1988]. Two pairs of moorings are selected for further analysis, each in a comparable water depth and with the lowest instrument at a comparable distance to the bottom. The first, upper slope pair (FS-1 and 411-2) is approximately on an isobath (~1000 m) which farther south crosses the Jan Mayen Fracture Zone and then turns eastward along the Greenland-Scotland Ridge (Figure 1). The second, lower slope pair (FS-3 and 412-4) is approximately on an isobath (~2000 m) which turns eastward at the Jan Mayen Fracture Zone. Values of the along-isobath component of the depth-averaged velocity, $\overline{\mathbf{u}}$ (here and henceforth the overbar denotes vertical averaging from the ocean bottom to the ocean surface), the near-bottom velocity, $\mathbf{u}_b$, and their difference, $\overline{\mathbf{u}}_r$, for the upper and lower slope pair of moorings are given in Table 1. The table also contains estimates of the along-slope transport ($M = \int \overline{v} H dx$, $M_b = \int v_b H dx$, and $M_r = M - M_b$) between the ~1000 and ~2000 m isobaths at 79°N and 75°N. In the north, the transports are obtained by integration of the along-slope flow from mooring FS-1 to mooring FS-3 (Figure 2a). In the south, the along-slope flow is integrated from mooring 411-2 to mooring 412-4 (Figure 2c) and multiplied by a factor of 0.7 (cosine of the average angle between meridians and isobaths) to account for the non-meridional run of the EGS at 75°N.

[9] The velocity distributions demonstrate that the along-isobath flow on the EGS is generally much larger than the corresponding cross-isobath flow, especially at 75°N where v (Figure 2c) exceeds u (Figure 2d) by an order of magnitude throughout the entire water column. At 79°N, the disproportion between the magnitude of v (Figure 2a) and u (Figure 2b) is not so large, especially in the upper layer at the two easternmost moorings because of the westward flow in the RAC. As a result of a small ratio of the u- and v-component of the near-bottom flow (~0.05 at 75°N and ~0.2 at 79°N), the estimates of v_b in Table 1 are actually the same as the observed velocities of bottom currents given originally by *Woodgate et al.* [1999] and *Foldvik et al.* [1988]. Even though the cross-isobath bottom flow is small, it may provide a significant term to the vorticity balance of the EGC [e.g., *Schlichtholz*, 2005]. Here we focus on the along-isobath component of $\mathbf{u}_b$ which, on both sections, is extreme at moorings on the ~1000 m isobath. On that isobath v_b increases from 2.6 cm s^{-1} at 79°N to 11.5 cm s^{-1} at 75°N, i.e., by $\Delta v_b \approx 9$ cm s^{-1}. The corresponding increase for the along-isobath component of $\overline{\mathbf{u}}$ is larger ($\Delta \overline{v} \approx 16$ cm s^{-1}) because of an increase of $\overline{v}_r$ from 0.2 cm s^{-1} to 7.2 cm s^{-1}. On the ~2000 m isobath, v_b increases from 0.4 cm s^{-1} at 79°N to 10.8 cm s^{-1} at 75°N while $\overline{v}$ increases from 3.8 cm s^{-1} to 14 cm s^{-1}, so that $\Delta \overline{v} \approx \Delta v_b \approx 10$ cm s^{-1}. Practically the same results for velocity changes along the upper (lower) EGS, i.e., $\Delta v_b \approx 9$ cm s^{-1} (10 cm s^{-1}) and $\Delta \overline{v} \approx 16$ cm s^{-1} (11 cm s^{-1}), are obtained from the current observations interpolated along the zonal sections onto the 1000 and 2000 m isobaths at 79°N and 75°N (assuming that v_b and $\overline{v}$ on the 1000 m isobath at 79°N are equal to the corresponding values at FS-1).

[10] Downstream changes of $\overline{v}$ can be caused either by variations in the bottom slope with no transport changes or by a net mass exchange with adjacent areas. The topographic effect is not negligible in the EGC since the ratio of the cross-slope area between the 1000 m and 2000 m isobaths at 79°N and 75°N is ~2. However, this ratio can explain less than a half of the average velocity increase along the EGS. Nearly two-thirds of the increase should be linked to a change in the along-slope transport. Estimates of M based on the velocity integration between the selected moorings are equal to 2.7 Sv at 79°N and 4.6 Sv at 75°N (Table 1). The downstream change of M is therefore equal to ΔM = 1.9 Sv. This change is due to the transport associated with the bottom flow which increases from 1.2 Sv at 79°N to 3.3 Sv at 75°N, i.e., by ΔM_b = 2.1 Sv. The small negative difference of 0.2 Sv between ΔM and ΔM_b is certainly within the error of transport estimates based on low-resolution

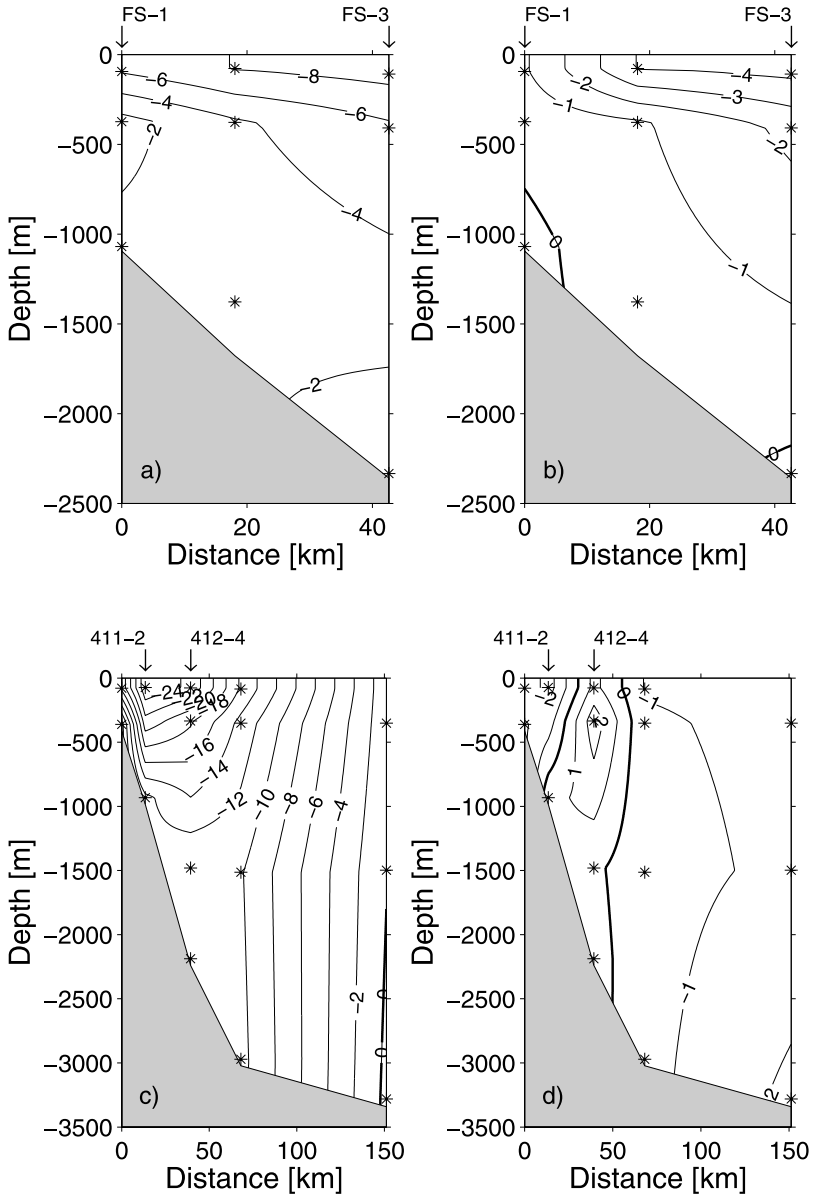

Figure 2. Vertical section of the velocity (in cm s^{-1}) in the EGC obtained from the current meters (stars) at moorings shown in Figure 1: (a) along-isobath component at 79°N; (b) cross-isobath component at 79°N; (c) along-isobath component at 75°N; and (d) cross-isobath component at 75°N. In Figures 2a and 2c, negative (positive) values indicate motion with a shallow (deep) water to the right. In Figures 2b and 2d, negative (positive) values indicate upslope (downslope) motion. Labeled arrows indicate moorings used for estimates of along-isobath flow in Table 1.

Table 1. Estimates of the Along-Isobath Velocity (v) and Along-Slope Transport (M) on the EGS at 79°N and 75°N From the Current Meter Data[a]

	∼1000 m isobath			∼2000 m isobath			Transport (∼1000–2000 m isobaths)			
Velocity	79°N	75°N	Δ	79°N	75°N	Δ		79°N	75°N	Δ
$\overline{v}$	−2.8	−18.7	(15.9)	−3.8	−14.0	(10.2)	M	−2.7	−4.6	(1.9)
v_b	−2.6	−11.5	(8.9)	−0.4	−10.8	(10.4)	M_b	−1.2	−3.3	(2.1)
$\overline{v}_r$	−0.2	−7.2	(7.0)	−3.4	−3.2	(−0.2)	M_r	−1.5	−1.3	(−0.2)

[a] v is in cm s^{-1} while M is in 10^6 m^3 s^{-1} (sign convention as in Figures 2a and 2c). v on the ∼1000 (∼2000) m isobath represents values measured at moorings FS-1 and 411-2 (FS-3 and 412-4) indicated by arrows in Figure 2a and 2c. M is is obtained by integration of the flow at 79°N (75°N) between moorings FS-1 and FS-3 (411-2 and 412-4). The overbar denotes vertical averaging while indices b and r indicate the bottom flow and the flow relative to the bottom, respectively. Δ stands for the difference (given in parenthesis) between values at 79°N and 75°N.

and 'non-synoptic' data. Estimates of the transport between the 1000 and 2000 m isobaths based on the interpolated velocities yield comparable results, with ΔM (=2.1 Sv) slightly exceeding ΔM_b (=1.8 Sv).

3. Basic Formulae for Geostrophic Currents

[11] Good approximations to the horizontal and vertical components of the momentum equation for ocean currents away from boundary layers and equator are the geostrophic and hydrostatic balances,

$$f\hat{\mathbf{z}} \times \mathbf{u}_g = -\frac{\nabla p}{\rho_0}, \tag{1}$$

and

$$\frac{\partial p}{\partial z} = -g\rho, \tag{2}$$

where $f \equiv$ Coriolis parameter, $g \equiv$ acceleration due to gravity, $z \equiv$ vertical coordinate (positive upward), $\hat{\mathbf{z}} \equiv$ vertical unit vector, $\nabla \equiv$ horizontal gradient operator, $\rho_0 \equiv$ constant density, $\rho \equiv$ density anomaly with respect to a depth-dependent reference density $\rho_r(z)$, $p \equiv$ pressure anomaly with respect to the static distribution associated with ρ_r, and $\mathbf{u}_g \equiv$ geostrophic velocity, i.e., horizontal velocity driven by the horizontal pressure gradient.

3.1. Geostrophic Velocity

[12] Various decompositions of the geostrophic velocity can be obtained by combining equations (1) and (2). For instance, integration of the latter upwards from the bottom ($z = -H$) to a given level z and insertion of the result into the former yields

$$\mathbf{u}_g = \mathbf{u}_\rho(x,y,z) + \mathbf{u}_\Phi(x,y) \equiv \frac{g}{f\rho_0}\left(\nabla \int_{-H}^{z} \rho dZ\right) \times \hat{\mathbf{z}} + \hat{\mathbf{z}} \times \frac{\nabla\Phi}{f\rho_0}, \tag{3}$$

where $\Phi \equiv p|_{z=-H}$ is the bottom pressure anomaly. Equation (3) is, for instance, a frictionless limit of equation (6) by *Schlichtholz and Houssais* [1999c]. It separates the dependence of the geostrophic flow on the local density distribution (contribution $\mathbf{u}_\rho$) from the dependence on external and remote factors affecting the bottom pressure distribution (contribution $\mathbf{u}_\Phi$). The velocity $\mathbf{u}_\rho$ is depth-dependent while the velocity $\mathbf{u}_\Phi$ is depth-independent.

[13] An important feature of the density-dependent flow is that it has a depth-independent contribution, hereafter referred to as the slope velocity ($\mathbf{u}_{\rho b}$). The slope velocity appears wherever the bottom slope ($s = |\nabla H|$) and the bottom density anomaly ($\rho_b \equiv \rho|_{z=-H}$) are both different from zero. This follows from the rule of interchange between the differential and integral operators applied to the formula for $\mathbf{u}_\rho$ in equation (3) which gives

$$\mathbf{u}_\rho = \mathbf{u}_{gr}(x,y,z) + \mathbf{u}_{\rho b}(x,y) \equiv \frac{g}{f\rho_0}\int_{-H}^{z} \nabla\rho \times \hat{\mathbf{z}} dZ + \frac{g}{f\rho_0}\rho_b \nabla H \times \hat{\mathbf{z}}. \tag{4}$$

The formula for $\mathbf{u}_{gr}$ (geostrophic velocity relative to zero flow at the bottom) appearing in equation (4) is classically obtained by upward integration of the thermal wind equation. The latter is derived by cross-differentiation of equations (1) and (2), and hence relates the vertical shear of $\mathbf{u}_g$ to the horizontal density gradient. While $\mathbf{u}_{gr}$ can have both cross- and along-isobath components, $\mathbf{u}_{\rho b}$ is aligned with isobaths as emphasized by *Walin et al.* [2004] and *Nilsson et al.* [2005]. In topography following coordinates we have

$$u_{\rho b} = 0, \qquad v_{\rho b} = -\frac{gs}{f\rho_0}\rho_b \equiv \alpha\rho_b, \tag{5}$$

where $v_{\rho b}$ is positive (negative) if the deep water is to the right (left) when looking downstream while $\alpha \equiv -gs(f\rho_0)^{-1}$ combines the dependence of $v_{\rho b}$ on the bottom slope and the Coriolis parameter.

[14] By inserting the decomposition of $\mathbf{u}_\rho$ from equation (4) into equation (3), one obtains

$$\mathbf{u}_g = \mathbf{u}_{gr} + \mathbf{u}_{\rho b} + \mathbf{u}_\Phi, \tag{6}$$

or, in the full version,

$$\mathbf{u}_g = \frac{g}{f\rho_0}\int_{-H}^{z} \nabla\rho \times \hat{\mathbf{z}} dZ + \frac{g}{f\rho_0}\rho_b \nabla H \times \hat{\mathbf{z}} + \hat{\mathbf{z}} \times \frac{\nabla\Phi}{f\rho_0}. \tag{7}$$

[15] Equation (7) is an equivalent of equation (9) in *Walin et al.* [2004] or equation (10) in *Nilsson et al.* [2005]. It shows that the constant of integration of the thermal wind equation, the bottom geostrophic velocity ($\mathbf{u}_{gb} \equiv \mathbf{u}_g|_{z=-H}$), is equal to the sum of $\mathbf{u}_{\rho b}$ and $\mathbf{u}_\Phi$, i.e.,

$$\mathbf{u}_{gb}(x,y) = \frac{g}{f\rho_0}\rho_b \nabla H \times \hat{\mathbf{z}} + \hat{\mathbf{z}} \times \frac{\nabla\Phi}{f\rho_0}. \tag{8}$$

[16] This formula for $\mathbf{u}_{gb}$ can also be obtained directly from equations (1) and (2) evaluated at $z = -H$ [e.g., *Rattray*, 1982; *Marshall*, 1995; *Schlichtholz*, 2002; *Schlichtholz*, 2004; *Schlichtholz*, 2005].

[17] It should be noted that the decomposition in equation (8) is not unique as ρ_b depends on the reference density ($\rho_r|_{z=-H}$). For instance, adding a constant $\Delta\rho$ to $\rho_r(z)$ results in a local change of $v_{\rho b}$ by the value of the product of α and $\Delta\rho$. The change requires a compensation of the same magnitude but opposite sign in v_Φ since v_{gb} does not depend on the choice of ρ_r. However, the difference between $v_{\rho b}$ at two points (say B and A) on the same isobath can be determined from hydrographic data with less ambiguity than $v_{\rho b}$ itself. The formula for $\Delta v_{\rho b}(B, A) \equiv v_{\rho b}(B) - v_{\rho b}(A)$ obtained from equation (5) is

$$\Delta v_{\rho b} = \alpha_c \Delta\rho_b + \rho_c \Delta\alpha \approx \alpha_c \Delta\rho_b, \tag{9}$$

where $\Delta\rho_b \equiv \rho_b(B) - \rho_b(A)$ is the bottom density difference between the points of interest, $\Delta\alpha \equiv \alpha(B) - \alpha(A)$ is the corresponding difference for the environmental parameter α, while ρ_c (α_c) is the average value of ρ_b (α) at B and A. Only the second contribution to $\Delta v_{\rho b}$ in equation (9), $\rho_c\Delta\alpha$, depends on the reference density. This contribution will always be zero if α is the same at B and A. It will be zero also if the average density at these points is chosen as

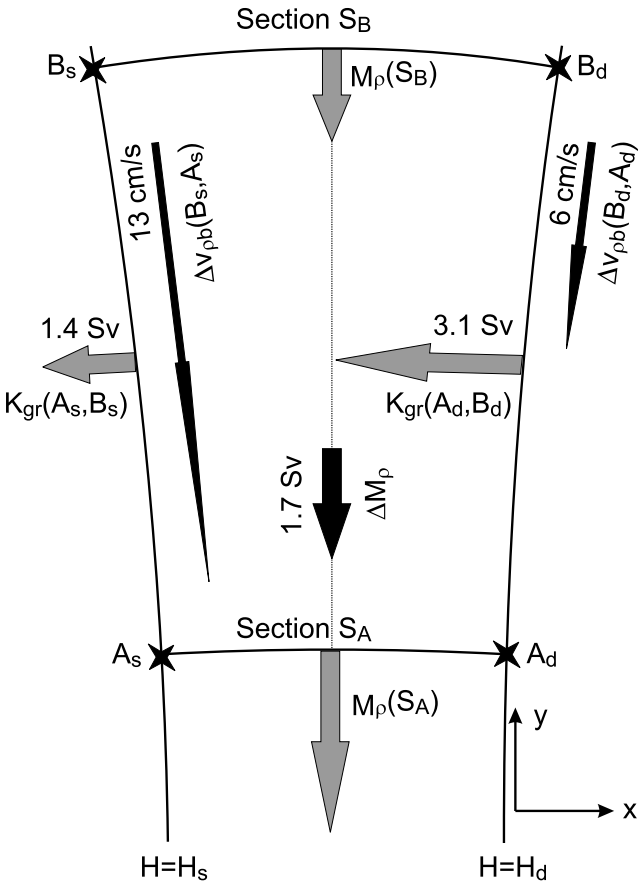

Figure 3. Schematic representation of the mass balance for the density-dependent flow over a sloping ocean bottom on the *f*-plane expressed by equation (14). The gray thick arrows attached to the line segments $A_s - B_s$ and $A_d - B_d$ indicate the direction and relative magnitude of the transport K_{gr} across a shallower (H_s = 1000 m) and deeper (H_d = 2000 m) isobath of the EGS between 75°N and 79°N obtained from the potential energy distribution in Figure 7. The gray thick arrows attached to the line segments $A_s - A_d$ and $B_s - B_d$ represent the transport M_ρ on the EGS across the southern (S_A at 75°N) and northern (S_B at 79°N) section. The vectors M_ρ are arbitrary, but their difference, indicated also by the black thick arrow ΔM_ρ, represents the direction and relative magnitude of the along-slope transport change inferred from the difference in K_{gr}. The thin arrows $\Delta v_{\rho b}$ indicate the direction and relative magnitude of the bottom velocity change along the EGS from 79°N to 75°N estimated from the bottom density distribution in Figure 6 using equation (9).

the reference density. The first contribution to $\Delta v_{\rho b}$ in equation (9), $\alpha_c \Delta\rho_b$, represents that part of the variation of v_{gb} which is uniquely determined by the local density field and can be used for diagnostic estimates.

3.2. Geostrophic Transport

[18] Vertical averaging of the relative velocity defined in equation (4) yields

$$\overline{\mathbf{u}}_{gr} = \hat{\mathbf{z}} \times \frac{\nabla\chi}{fH} - \frac{g}{f\rho_0}\rho_b \nabla H \times \hat{\mathbf{z}}, \tag{10}$$

where $\rho_0\chi \equiv g\int_{-H}^{0}\rho z dz$ is the anomaly of the potential energy per unit area. Similar formulae can be found, e.g., in the work of *Rattray* [1982] or *Schlichtholz and Houssais* [1999c]. The second term on the right-hand side (RHS) of equation (10) has the same magnitude but opposite sign to the slope velocity ($\mathbf{u}_{\rho b}$) from equation (4). Therefore the total density-dependent transport per unit width ($H\overline{\mathbf{u}}_\rho = H\overline{\mathbf{u}}_{gr} + H\mathbf{u}_{\rho b}$) is a function of the potential energy, but not the bottom density, i.e.,

$$H\overline{\mathbf{u}}_\rho = \hat{\mathbf{z}} \times \frac{\nabla\chi}{f}. \tag{11}$$

[19] Equation (11) implies that

$$\nabla \cdot \left(H\overline{\mathbf{u}}_\rho\right) = -\frac{H\overline{\mathbf{u}}_\rho}{f} \cdot \nabla f, \tag{12}$$

so that the density-dependent transport is nondivergent on an *f*-plane, i.e., for $f = f_c = const$.

[20] Since $\mathbf{u}_{\rho b}$ is aligned with isobaths, the along-isobath gradient of χ fully determines the cross-isobath relative transport ($H\overline{u}_{gr} = H\overline{u}_\rho$). This transport cumulated between any point y and a reference point $y = y_0$ on a given isobath is

$$K_{gr}(y, y_0) = \left[\frac{\chi}{f}(y) - \frac{\chi}{f}(y_0)\right] - \int_y^{y_0} \frac{\chi}{f^2}\frac{\partial f}{\partial y} dY. \tag{13}$$

[21] The last term on the RHS of equation (13) disappears on the *f*-plane. In that case the relative transport between points *A* and *B* on the same isobath depends only on the potential energy difference between these points, i.e., $K_{gr}(A, B) = f_c^{-1}[\chi(A) - \chi(B)]$.

[22] Consider the total density-dependent transport in a box limited by two isobaths, a shallower one ($H = H_s$) and a deeper one ($H = H_d$), and two cross-slope sections, say S_A and S_B. Let section S_B be located forward with respect to section S_A when looking in the direction with the deep water to the right (Figure 3). Section S_A intersects the shallower (deeper) isobath at point A_s (A_d) while section S_B intersects the shallower (deeper) isobath at point B_s (B_d). The nondivergence of $H\overline{\mathbf{u}}_\rho$ in this box can be written in the integral form on the *f*-plane as

$$\Delta M_\rho \equiv \Delta M_{\rho b} + \Delta M_{gr} = -\Delta K_{gr}, \tag{14}$$

where $\Delta K_{gr} \equiv K_{gr}(A_d, B_d) - K_{gr}(A_s,B_s)$ is the difference between relative transports across the deeper and shallower isobaths while $\Delta M_\rho \equiv M_\rho(S_B) - M_\rho(S_A)$ is the difference between density-dependent transports across sections S_B and S_A. Equation (14) can be used to estimate the change of the density-dependent along-slope transport (including the contribution $\Delta M_{\rho b}$ from the slope velocity) from values of χ at A_s, A_d, B_s, and B_d, or to estimate $\Delta M_{\rho b}$ from the imbalance of the relative transport ($\Delta K_{gr} + \Delta M_{gr}$). These estimates are independent of the reference density and the bottom slope.

4. Estimates of Geostrophic Flow From Hydrographic Data

[23] As already mentioned in the introduction, the density-dependent variables are calculated using the annual mean

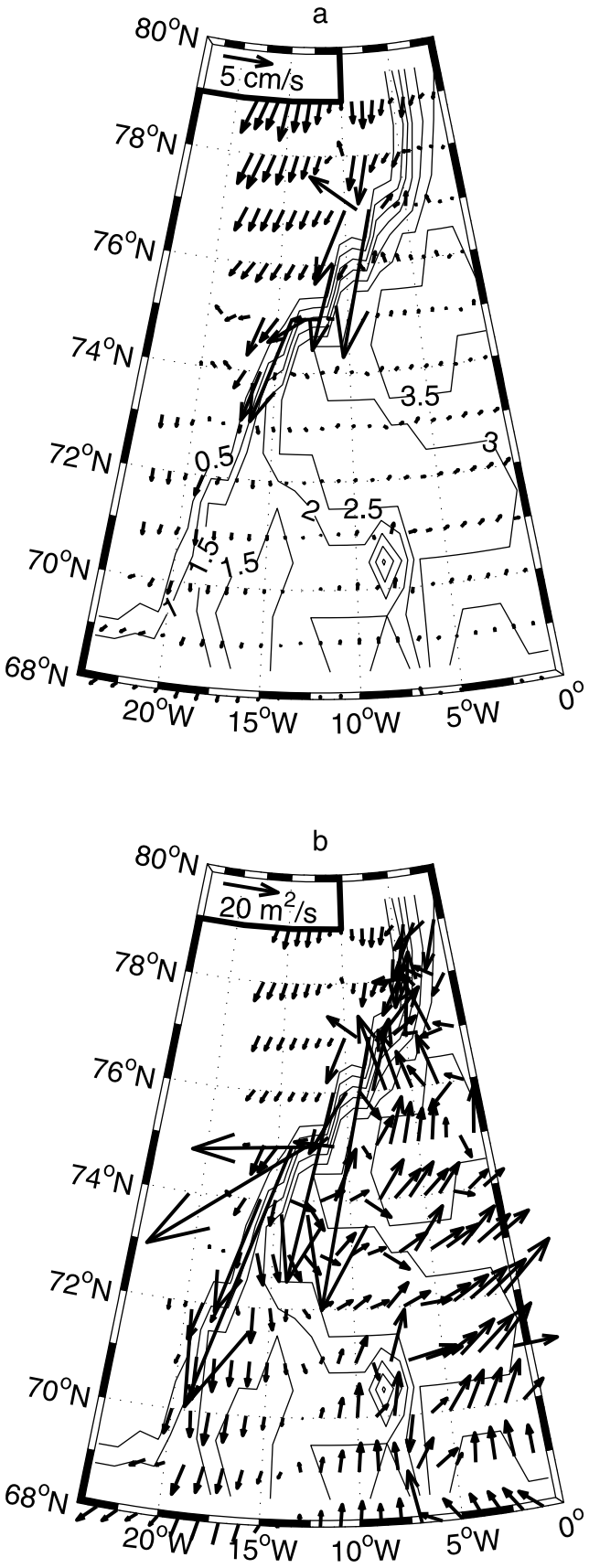

temperature and salinity from the PHC [*Steele et al.*, 2001]. The latter is a product of merging two data sets of objectively analyzed, heavily smoothed hydrographic fields. The PHC data are available on a 1° lon ×1° lat grid and have a vertical resolution decreasing with depth from 10 m in the upper 30 m layer to 500 m below the 2000 m level.

4.1. Relative Flow

[24] To estimate the relative geostrophic flow from equation (10), first χ and ρ_b are calculated at the PHC grid points. Then the zonal and meridional velocity components are estimated at half a distance between the adjacent grid points and interpolated onto a common 1° lon ×1° lat grid. The distribution of $\overline{\mathbf{u}}_{gr}$ obtained in the area west of the Greenwich meridian shows that a large vertically sheared flow in the EGC occurs on the shelf (Figure 4a). However, the largest relative transport ($H\overline{\mathbf{u}}_{gr}$) is concentrated on the EGS (Figure 4b).

[25] Distributions of the along-isobath component of $\overline{\mathbf{u}}_{gr}$, estimated by projecting the vectors from Figure 4a on the direction of local isobaths and then interpolated onto the 1000 and 2000 m isobaths, are shown in Figure 5. On the upper slope, the magnitude of $\overline{v}_{gr}$ increases from ~1 cm s^{-1} at 79°N to ~10 cm s^{-1} at 75°N (Figure 5, circles). The increase $\Delta\overline{v}_{gr} \approx 9$ cm s^{-1} is close to the corresponding estimate $\Delta\overline{v}_r = 7$ cm s^{-1} based on the current meter data (Table 1). On the lower slope, $\Delta\overline{v}_{gr}$ between 79°N and 75°N is negligible (Figure 5, crosses). This is also in agreement with the observations, although the values of $\overline{v}_{gr}$ at 79°N and 75°N (1–2 cm s^{-1}) are smaller than the corresponding estimates of $\overline{v}_r$ from the current meter data (~3 cm s^{-1}).

4.2. Slope Velocity

[26] As pointed out in the introduction and further discussed in section 3.1, a suitable variable for studying variations of the density-dependent contribution to the bottom geostrophic velocity is the bottom density. Distributions of ρ_b on the EGS along the 1000 and 2000 m isobaths (Figure 6a) are obtained by an interpolation of the PHC data followed by a slight along-isobath smoothing intended to suppress point-to-point fluctuations. On both isobaths, ρ_b shows a southward densification from Fram Strait to a maximum at ~75°N and then a southward rarification. According to equation (5), such a distribution corresponds to a slope velocity maximum at ~75°N. The bottom density difference between 79°N and 75°N is $\Delta\rho_b = -0.04$ kg m^{-3} on the upper slope (Figure 6a, circles) and $\Delta\rho_b = -0.02$ kg m^{-3} on the lower slope (Figure 6a, crosses). The bottom density decrease along the 1000 m isobath south of 75°N toward Denmark Strait is as large as the corresponding increase from Fram Strait to 75°N.

[27] The slope velocity depends not only on ρ_b, but also on the bottom slope and the Coriolis parameter. Variation of the latter are small in the area considered. For instance,

Figure 4. Distribution of the relative geostrophic flow in the area of the EGC obtained from the PHC climatology using equation (10): (a) the depth-averaged velocity, $\overline{\mathbf{u}}_{gr}$; and (b) the transport per unit width, $H\overline{\mathbf{u}}_{gr}$. The isolines represent the bottom topography (with the increment of 0.5 km) used in the calculations.

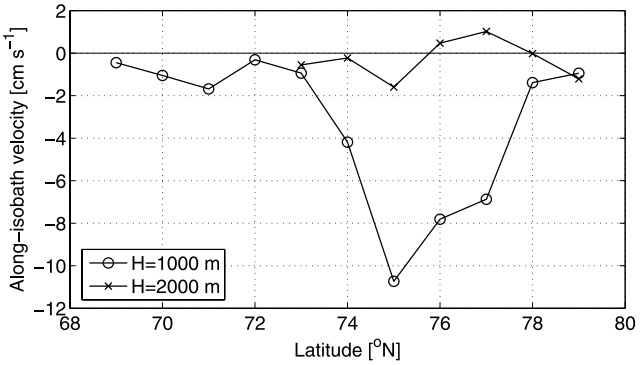

Figure 5. Distribution of the along-isobath component of the depth-averaged relative geostrophic velocity on the 1000 m (circles) and 2000 m (crosses) isobath along the EGS obtained from the PHC climatology by an interpolation of local estimates of the along-isobath component of the velocity vectors from Figure 4a. The sign convention is the same as in Figure 2a.

the relative departure of f from a constant value ($f_c = 1.4 \times 10^{-4}$ s^{-1}) between 75°N and 79°N is only 2%. Of course, the bottom slope varies more. Distributions of s on the EGS along the 1000 and 2000 m isobaths (Figure 6b) are obtained from the ETOPO5 data. The average value of the slope at 75°N and 79°N is $s_c = 0.05$ on the 1000 m isobath and $s_c = 0.04$ on the 2000 m isobath. These values can be combined with the estimates of $\Delta\rho_b$ made above and other parameters ($\rho_0 = 1027$ kg m^{-3} and $g = 9.8$ m s^{-2}) to yield estimates of the slope velocity change between 79°N and 75°N based on the contribution $\alpha_c\Delta\rho_b$ to $\Delta v_{\rho b}$ in equation (9). One obtains $\alpha_c\Delta\rho_b = 13$ cm s^{-1} for the upper slope and $\alpha_c\Delta\rho_b = 6$ cm s^{-1} for the lower slope. These values are close to the estimates of the bottom velocity change (Δv_b) from the current meter data (Table 1). On the lower slope $\alpha_c\Delta\rho_b$ is 40% smaller than Δv_b while on the upper slope it is 45% larger than Δv_b.

4.3. Density-Dependent Transport

[28] As discussed in section 3.2, a suitable variable for studying variations of the density-dependent geostrophic transport is the potential energy. Distributions of $\rho_0\chi$ interpolated from the PHC grid onto the 1000 and 2000 m isobaths of the EGS are shown in Figure 7a. On both isobaths, $\rho_0\chi$ decreases from Fram Strait to ~75°N and then increases farther south. As a consequence, the relative geostrophic flow across both isobaths is onshore from 79°N to ~75°N and offshore farther south. The onshore transport across the deeper isobath, cumulated between 75°N and 79°N using equation (13), is equal to 3.1 Sv (Figure 7b, crosses). The corresponding estimate for the transport across the shallower isobath is only 1.4 Sv (Figure 7b, circles). The difference ($\Delta K_{gr} = -1.7$ Sv) should be compensated by an increase of the density-dependent along-slope transport from 79°N to 75°N since variations of the Coriolis parameter are negligible. Equation (14) then yields $\Delta M_\rho = 1.7$ Sv. This value is very close (to within 0.2 Sv) to the increase ΔM of the total along-slope transport between the ~1000 and ~2000 m isobaths obtained from the current meter data (Table 1).

[29] The distribution of K_{gr} along a given isobath shows divergences and convergences of the density-dependent along-slope transport between this isobath and the coast, where $\chi = 0$. In particular, the distribution in Figure 7b (circles) indicates that the onshore relative geostrophic transport across the 1000 m isobath between 79°N and 75°N (equivalent downstream increase of M_ρ) is fully compensated by the corresponding offshore transport between 75°N and 69°N (equivalent downstream decrease of M_ρ).

5. Discussion With Concluding Remarks

[30] Since the ice cover shields a major portion of the EGC from the atmosphere [e.g., *Aagaard and Coachman*, 1968; *Mauritzen*, 1996b], the density distribution on the EGS should mainly be influenced by lateral exchanges with

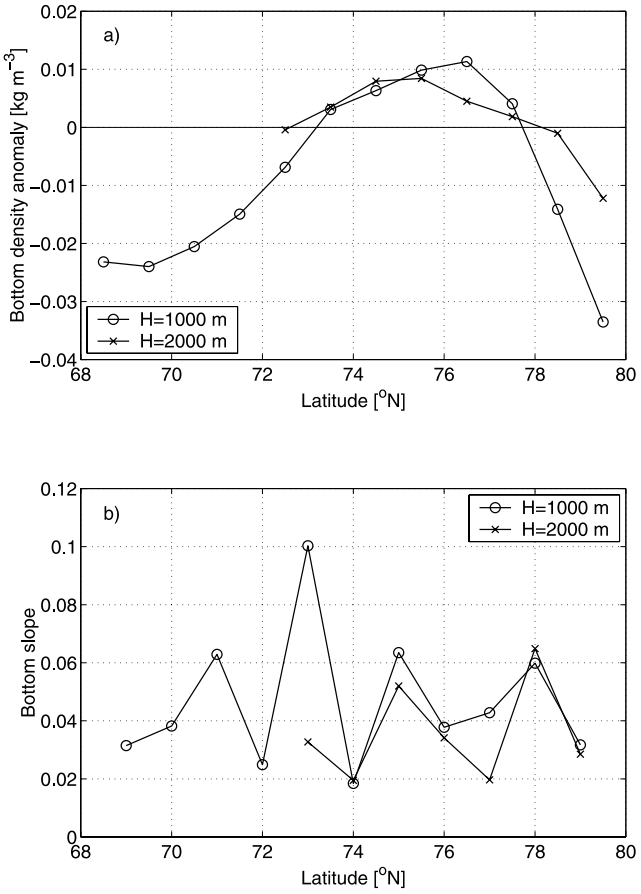

Figure 6. Distribution of variables determining the slope velocity in equation (5) on the 1000 m (circles) and 2000 m (crosses) isobaths along the EGS: (a) bottom density anomaly calculated from the PHC; and (b) bottom slope estimated from the ETOPO5. The anomalies in Figure 6a are calculated by an interpolation of the gridded values of the bottom density referenced to the density profile averaged over the entire area shown in Figure 4 and a subsequent along-isobath smoothing (3-points running mean). The slopes in Figure 6b are interpolated from the local values estimated on the 5-min grid and then subsampled in latitude.

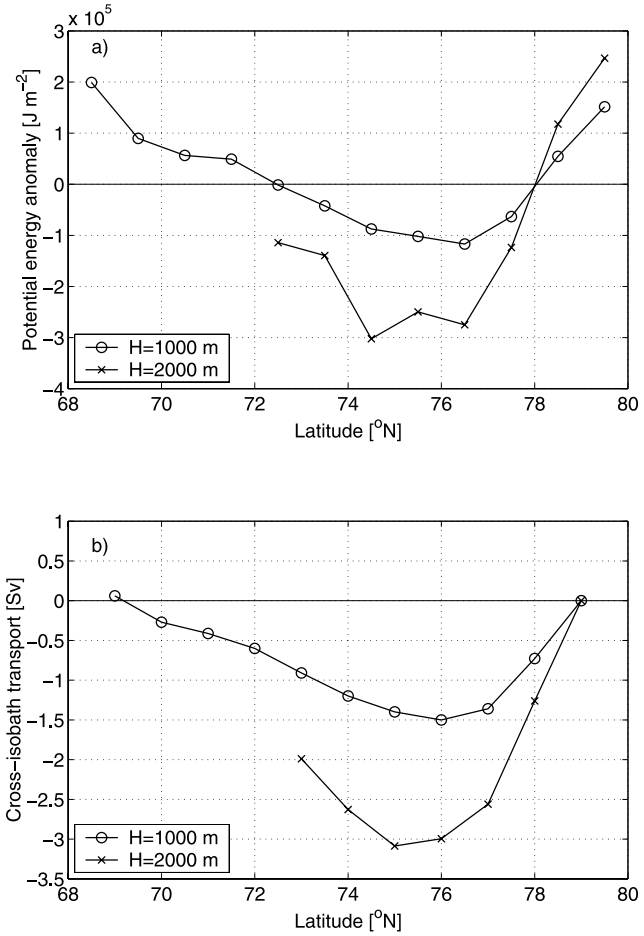

Figure 7. Distribution of (a) the anomaly of the potential energy per unit area along the EGS obtained from the PHC climatology by an interpolation of the gridded values onto the 1000 m (circles) and 2000 m (crosses) isobath; and (b) the associated cross-isobath component of the relative geostrophic transport cumulated southward from 79°N using equation (13). The anomalies in Figure 7a are calculated with respect to the potential energy of a reference density profile obtained by horizontal density averaging in the entire area shown in Figure 4. The sign convention in Figure 7b is the same as in Figure 2b.

deep basins. As already mentioned in the introduction, dense intermediate and deep water masses are formed in the Greenland Sea gyre and spread onto the EGS. One can therefore expect to find a local density maximum on the lower as well as upper EGS when looking in the along-isobath direction. A density maximum on the EGS at ~75°N has been evidenced in the present study using climatological distributions of the bottom density (Figure 6a) and potential energy (Figure 7a) based on the PHC data [*Steele et al.*, 2001]. These are important variables since their along-isobath variations determine the corresponding variations of the density-dependent part of the bottom geostrophic velocity and the along-slope variations of the total density-dependent transport as expressed by equations (9) and (14), respectively. The presence of dense waters on the EGS at ~75°N implies that the downstream feeding of the depth-independent along-isobath flow in the EGC by the depth-dependent cross-isobath (onshore) flow ceases at this latitude and that farther south it is the depth-independent flow which feeds the depth-dependent (offshore) flow. Moreover, a same magnitude of the bottom density change on the upper EGS from 75°N toward Fram Strait and Denmark Strait indicates that a significant difference in the depth-independent flow between 79°N and 69°N, if exists, cannot be related to density variations. A corresponding compensation in the potential energy change further demonstrates that the transport variations in the EGC between 79°N and 69°N are part of a density-dependent internal cyclonic circulation in the Nordic Seas.

[31] A check against long-term current observations on the EGS at 79°N from *Foldvik et al.* [1988] and 75°N from *Woodgate et al.* [1999] has revealed that the along-isobath density variations are indeed relevant for the dynamics of the EGC. The current meter data yield an estimate for the downstream bottom velocity increase equal to ~9 and ~10 cm s^{-1} along the 1000 and 2000 m isobath, respectively (Table 1). The corresponding geostrophic estimates based on the bottom density change are higher on the upper slope and lower on the lower slope (Figure 3), but their average value perfectly fits the observations. Similarly, a very good agreement is found between estimates of the downstream transport increase between the 1000 and 2000 m isobaths. The total increase of ~2 Sv obtained from the current measurements is mainly associated with the bottom flow. The corresponding transport increase calculated from the potential energy distribution is lower only by ~15%. Such a good agreement may seem somehow fortuitous given the nonsynopticity of the data and sampling errors. However, all estimates are consistent. Even the differences between the southward bottom velocity increase on the individual isobaths obtained from the current and bottom density data can be explained by the geostrophic dynamics. If interpreted as changes of the flow associated with the bottom pressure distribution, they represent a southward increase of this flow on the 2000 m isobath and a northward increase on the 1000 m isobath, both equal to ~4 cm s^{-1}. The associated transport increase should be small and southward as obtained by the difference between the estimates from the current meter and potential energy data.

[32] **Acknowledgments.** The author acknowledges the Polar Science Center (Seattle, Washington, United States) for providing the hydrographic data and the Academic Computer Center in Gdansk TASK for computational support. Reviewers comments helped to improve the presentation greatly.

References

Aagaard, K. (1970), Wind-driven transports in the Greenland and Norwegian seas, *Deep Sea Res.*, *17*, 281–291.

Aagaard, K., and L. K. Coachman (1968), The East Greenland Current north of Denmark Strait: Part I, *Arctic*, *21*, 181–200.

Aagaard, K., J. H. Swift, and E. C. Carmack (1985), Thermohaline circulation in the Arctic Mediterranean Seas, *J. Geophys. Res.*, *90*(C5), 4833–4846.

Aagaard, K., E. Fahrbach, J. Meincke, and J. H. Swift (1991), Saline outflow from the Arctic Ocean: Its contribution to the deep waters of the Greenland, Norwegian, and Iceland Seas, *J. Geophys. Res.*, *96*, 4833–4846.

Csanady, G. T. (1988), Ocean currents over the continental slope, *Adv. Geophys.*, *30*, 95–203.

Fahrbach, E., J. Meincke, S. Østerhus, G. Rohardt, U. Schauer, V. Tverberg, and J. Verduin (2001), Direct measurements of volume transports through Fram Strait, *Polar Res.*, *20*, 217–224.

Foldvik, A., K. Aagaard, and T. Torresen (1988), On the velocity field of the East Greenland Current, *Deep Sea Res.*, *35*, 1335–1354.
Gordon, A. L. (1986), Interocean exchange of thermocline water, *J. Geophys. Res.*, *91*(C4), 5037–5046.
Hansen, B., and S. Østerhus (2000), North Atlantic - Nordic Seas exchanges, *Prog. Oceanogr.*, *45*, 109–208.
Jakobsen, P. K., M. H. Ribergaard, D. Quadfasel, T. Schmith, and C. W. Hughes (2003), Near-surface circulation in the northern North Atlantic as inferred from Lagrangian drifters: Variability from mesoscale to interannual, *J. Geophys. Res.*, *108*(C8), 3251, doi:10.1029/2002JC001554.
Jónsson, S. (1991), Seasonal and interannual variability of wind stress curl over the Nordic Seas, *J. Geophys. Res.*, *96*(C2), 2649–2659.
Marshall, D. (1995), Influence of topography on the large-scale ocean circulation, *J. Phys. Oceanogr.*, *25*, 1622–1635.
Mauritzen, C. (1996a), Production of dense overflow waters feeding the North Atlantic across the Greenland-Scotland Ridge. Part 1: Evidence of a revised circulation scheme, *Deep Sea Res., Part I*, *43*, 769–806.
Mauritzen, C. (1996b), Production of dense overflow waters feeding the North Atlantic across the Greenland-Scotland Ridge. Part 2: An inverse model, *Deep Sea Res., Part I*, *43*, 807–835.
Metclaf, W. G. (1960), A note on water movement in the Greenland and Norwegian Seas, *Deep Sea Res.*, *7*, 190–200.
Nilsson, J., G. Walin, and G. Broström (2005), Thermohaline circulation induced by bottom friction in sloping-boundary basins, *J. Mar. Res.*, *63*, 705–728.
Nøst, O. A., and P. E. Isachsen (2003), The large-scale time-mean ocean circulation in the Nordic Seas and the Arctic Ocean estimated from simplified dynamics, *J. Mar. Res.*, *61*, 175–210.
Orvik, K. A., Ø. Skagseth, and M. Mork (2001), Atlantic inflow to the Nordic Seas: current structure and volume fluxes from moored current meters, VM-ADCP and SeaSoar-CTD observations, 1995–1999, *Deep Sea Res., Part I*, *48*, 937–957.
Park, Y.-H., and J. M. Guernier (2001), A simple method for diagnosing the bottom current field of the world's oceans, *J. Phys. Oceanogr.*, *31*, 972–991.
Rattray, M. (1982), A simple exact treatment of the baroclinicity-bathymetry interaction in a frictional, iterative, diagnostic ocean model, *J. Phys. Oceanogr.*, *12*, 997–1003.
Rudels, B., E. Fahrbach, J. Meincke, G. Budéus, and P. Eriksson (2002), The East Greenland Current and its contribution to the Denmark Strait overflow, *ICES J. Mar. Sci.*, *59*, 1133–1154.
Rudels, B., G. Björk, J. Nilsson, P. Winsor, I. Lake, and C. Nohr (2005), The interaction between waters from the Arctic Ocean and the Nordic Seas north of Fram Strait and along the East Greenland Current: Results from the Arctic Ocean-02 Oden expedition, *J. Mar. Sys.*, *55*, 1–30.
Schauer, U., E. Fahrbach, S. Østerhus, and G. Rohardt (2004), Arctic warming through Fram Strait: Oceanic heat transport from 3 years of measurements, *J. Geophys. Res.*, *109*, C06026, doi:10.1029/2003JC001823.
Schlichtholz, P. (2002), On a modified arrested topographic wave in Fram Strait, *J. Geophys. Res.*, *107*(C11), 3189, doi:10.1029/2001JC000799.
Schlichtholz, P. (2004), Correction to "On a modified arrested topographic wave in Fram Strait", *J. Geophys. Res.*, *109*, C09006, doi:10.1029/2004JC002582.
Schlichtholz, P. (2005), Climatological baroclinic forcing of the barotropic flow in the East Greenland Current in Fram Strait, *J. Geophys. Res.*, *110*, C08013, doi:10.1029/2004JC002701.
Schlichtholz, P., and M.-N. Houssais (1999a), An inverse modeling study in Fram Strait. Part I: Dynamics and circulation, *Deep Sea Res., Part II*, *46*, 1083–1135.
Schlichtholz, P., and M.-N. Houssais (1999b), An inverse modeling study in Fram Strait. Part II: Water mass distribution and transports, *Deep Sea Res., Part II*, *46*, 1137–1168.
Schlichtholz, P., and M.-N. Houssais (1999c), An investigation of the dynamics of the East Greenland Current in Fram Strait based on a simple analytical model, *J. Phys. Oceanogr.*, *29*, 2240–2265.
Shaw, P.-T., and G. T. Csanady (1983), Self-advection of density perturbations on a sloping continental shelf, *J. Phys. Oceanogr.*, *13*, 769–782.
Steele, M., R. Morley, and W. Ermold (2001), PHC: A global ocean hydrography with a high-quality Arctic Ocean, *J. Climate*, *14*, 2079–2087.
U.S. National Geophysical Data Center (1988), *5-minute gridded global relief data topography data set (ETOPO5) [CD-ROM]*, http://www.ngdc.noaa.gov/mgg/fliers/93mgg01.html, Boulder, Colo.
Walin, G., G. Broström, J. Nilsson, and O. Dahl (2004), Baroclinic boundary currents with downstream decreasing buoyancy: A study of an idealized Nordic Seas system, *J. Mar. Res.*, *62*, 517–543.
Woodgate, R. A., E. Fahrbach, and G. Rohardt (1999), Structure and transports of the East Greenland Current from moored current meters, *J. Geophys. Res.*, *104*(C8), 18,059–18,072.
Wunsch, C. (1996), *The Ocean Circulation Inverse Problem*, 442 pp., Cambridge Univ. Press, New York.

P. Schlichtholz, Institute of Oceanology, Polish Academy of Sciences, Powstancow Warszawy 55, 81-712 Sopot, Poland. (schlicht@iopan.gda.pl)